Burns & Trauma, 2023, 11, tkad035
https://doi.org/10.1093/burnst/tkad035
Research Article

OXFORD

Research Article

Peptide RL-QN15 promotes wound healing of diabetic foot ulcers through p38 mitogen-activated protein kinase and smad3/miR-4482-3p/vascular endothelial growth factor B axis

Dandan Sun[1,†], Kun Guo[1,†], Naixin Liu[1], Yilin Li[1], Yuansheng Li[1], Yan Hu[1], Shanshan Li[1], Zhe Fu[1], Yinglei Wang[1], Yutong Wu[1], Yingxuan Zhang[1], Jiayi Li[1], Chao Li[2], Zhuo Wang[2], Zijian Kang[1], Jun Sun[1,*], Ying Wang[3,*] and Xinwang Yang[1,*]

[1]Department of Anatomy and Histology and & Embryology, Faculty of Basic Medical Science, Kunming Medical University, No. 1168 Chunrong West Road, Chenggong District, Kunming, 650500, Yunnan, China, [2]Department of Biochemistry and Molecular Biology, Faculty of Basic Medical Science, Kunming Medical University, No. 1168 Chunrong West Road, Chenggong District, Kunming, 650500, Yunnan, China and [3]Key Laboratory of Chemistry in Ethnic Medicinal Resources & Key Laboratory of Natural Products Synthetic Biology of Ethnic Medicinal Endophytes, State Ethnic Affairs Commission & Ministry of Education, School of Ethnic Medicine, Yunnan MinZu University, No. 2929 Yuehua Street, Chenggong District, Kunming, 650504, Yunnan, China

*Correspondence. Xinwang Yang, Email: yangxinwanghp@163.com; Ying Wang, Email: wangying_814@163.com; Jun Sun, Email: sunjun6661@126.com

[†]Dandan Sun and Kun Guo contributed equally to this work.

Received 2 December 2022; Revised 31 March 2023; Accepted 18 June 2023

Abstract

Background: Wound management of diabetic foot ulcers (DFUs) is a complex and challenging task, and existing strategies fail to meet clinical needs. Therefore, it is important to develop novel drug candidates and discover new therapeutic targets. However, reports on peptides as molecular probes for resolving issues related to DFUs remain rare. This study utilized peptide RL-QN15 as an exogenous molecular probe to investigate the underlying mechanism of endogenous non-coding RNA in DFU wound healing. The aim was to generate novel insights for the clinical management of DFUs and identify potential drug targets.

Methods: We investigated the wound-healing efficiency of peptide RL-QN15 under diabetic conditions using *in vitro* and *in vivo* experimental models. RNA sequencing, *in vitro* transfection, quantitative real-time polymerase chain reaction, western blotting, dual luciferase reporter gene detection, *in vitro* cell scratches, and cell proliferation and migration assays were performed to explore the potential mechanism underlying the promoting effects of RL-QN15 on DFU repair.

Results: Peptide RL-QN15 enhanced the migration and proliferation of human immortalized keratinocytes (HaCaT cells) in a high-glucose environment and accelerated wound healing in a DFU rat model. Based on results from RNA sequencing, we defined a new microRNA (miR-4482-3p) related to the promotion of wound healing. The bioactivity of miR-4482-3p was verified by inhibiting and overexpressing miR-4482-3p. Inhibition of miR-4482-3p enhanced the migration and proliferation

ability of HaCaT cells as well as the expression of vascular endothelial growth factor B (VEGFB). RL-QN15 also promoted the migration and proliferation ability of HaCaT cells, and VEGFB expression was mediated via inhibition of miR-4482-3p expression by the p38 mitogen-activated protein kinase (p38MAPK) and smad3 signaling pathways.

Conclusions: RL-QN15 is an effective molecule for the treatment of DFUs, with the underlying mechanism related to the inhibition of miR-4482-3p expression via the p38MAPK and smad3 signaling pathways, ultimately promoting re-epithelialization, angiogenesis and wound healing. This study provides a theoretical basis for the clinical application of RL-QN15 as a molecular probe in promoting DFU wound healing.

Key words: RL-QN15, Diabetic foot ulcer, Wound healing, miR-4482-3p, Vascular endothelial growth factor B, Peptide, Mitogen-activated protein kinase

Highlights

- RL-QN15 was used as an exogenous molecular probe for wound healing treatment of DFUs.
- RL-QN15 markedly promoted DFU skin wound repair.
- miR-4482-3p, a novel microRNA, was an effective target for promoting DFU repair.

Background

At present, ~537 million people are living with diabetes worldwide, and this number is projected to reach 783 million by 2045 [1]. Diabetic patients have a 25% lifetime risk of developing foot ulcers. As a common and potentially severe complication, diabetic foot ulcers (DFUs) can seriously affect quality of life and even endanger the lives of those affected [2–4]. Despite extensive research exploring therapeutic mechanisms and interventions for DFUs, clinical outcomes remain poor [5–7].

DFU wound healing involves multiple complex regulatory mechanisms, such as cell migration and proliferation and secretion of vascular growth factors. As the most important cell type in the skin, keratinocytes restore the epidermal barrier through migration, proliferation and differentiation, and execute the re-epithelialization process [8–11]. Keratinocytes are involved in angiogenesis of diabetic wounds [12,13], a critical process in healing [14–16]. Vascular endothelial growth factor B (VEGFB), a member of the VEGF family, promotes angiogenesis in wound healing [17–19]. However, in chronic diabetic wounds, keratinocytes show decreased migration and proliferation ability and decreased secretion of VEGF, potentially significant pathophysiological changes in chronic diabetic skin during wound healing [20–22].

MicroRNAs (miRNAs) are small, highly conserved endogenous non-coding RNA molecules involved in a variety of biological processes, including diabetic wound healing [23]. miRNAs play important roles in many physiological and pathological aspects by activating certain signaling pathways and down-regulating or up-regulating certain genes [24,25]. Many studies have shown that miRNAs can be used as therapeutic targets to improve chronic DFUs. For example, miRNA-129 and -335 promote diabetic wound healing by inhibiting the expression of MMP-9 [26], and miRNA-21-3p accelerates diabetic wound healing by down-regulating SPRY1 [27].

The functional diversity and structural stability of peptides have been extensively studied in recent years [28–31]. For example, the discovery of insulin was a breakthrough in the treatment of diabetes [32]. Exenatide has also been shown to improve glycemic control in patients with type 2 diabetes and is now being studied for the treatment of Parkinson's disease and other disorders [33]. Therefore, peptides can serve as effective and viable lead molecules for drug discovery, often leading to the development of peptide drugs with high selectivity and specificity.

Our group previously identified a peptide RL-QN15, which was shown to accelerate wound healing in mice [34]. The discovery of this peptide and our extensive studies suggest that RL-QN15 is a potential drug lead molecule for promoting wound healing [35–37]. Using active peptides as exogenous molecular probes to identify novel endogenous molecular targets of disease is an important approach in modern biology [38–41]. To date, however, only one exogenous molecular probe specific to trauma repair has been investigated by our research group [42]. Therefore, further investigations of active peptides as molecular probes are required to explore the molecular targets of chronic refractory wounds, such as DFUs, and to provide potential molecular drugs and targeting strategies for DFU healing.

In the current study, we designed *in vitro* and *in vivo* experimental models to investigate the functional role of RL-QN15 in wound healing under diabetic conditions and to explore the potential mechanism underlying the regulatory effects of RL-QN15 on wound healing in DFUs. This study

should provide novel drug candidates and new therapeutic targets for the repair of DFUs.

Methods

Cell culture and treatment

Human immortalized keratinocytes (HaCaT cells) were purchased from the Cell Bank of the Kunming Institute of Zoology, Chinese Academy of Sciences. The HaCaT cells were seeded in Dulbecco's modified Eagle's medium (DMEM, Gibco, USA) without glucose, supplemented with 10% fetal bovine serum (Gibco, USA) and antibiotics (100 units/ml penicillin and 100 units/ml streptomycin) (Gibco, USA). For further experiments, the HaCaT cells were reseeded in high-glucose DMEM (25 mM D-glucose, Gibco, USA) for 48 h. All HaCaT cells were cultured at 37°C in a humidified incubator containing 5% CO_2, with the medium changed on alternate days.

Ethics approval and consent to participate

All animal procedures were conducted in accordance with the requirements of the Ethics Committee of Kunming Medical University, Yunnan Province, China (License number: kmmu2021118).

Preparation of RL-QN15

The RL-QN15 peptide ('QNSYADLWCQFHYMC') was produced by Wuhan Tiande Biotechnology Co., Ltd (Wuhan, China) via solid-phase synthesis to a purity >95%. RL-QN15 was dissolved in phosphate-buffered saline (PBS) to prepare different concentrations (100 pM, 1 nM and 10 nM) for subsequent experiments.

Cellular wound healing activity

The effect of RL-QN15 on HaCaT cell scratch repair activity under a high-glucose environment was examined using a cell scratch assay according to our previous study [37]. The cell scratch assay was also used to detect the influence of a miR-4482-3p mimic and inhibitor on cell scratch repair after transfection. Simply, the miR-4482-3p mimic, inhibitor and interfering miRNA (negative control, NC) were transfected for 48 h and the cell scratch assay was performed to detect cell repair activity. In addition, the cell scratch assay was used to detect the effect of RL-QN15 (10 nM) on reversing cell scratch repair after transfection with miR-4482-3p and NC mimics, with the miR-4482-3p and NC mimic groups without RL-QN15 (10 nM) used as NCs.

Cell proliferation viability

According to our previous study [36], the 3-(4, 5-dimethylthiazol-2-yl)-5-(3-carboxymethoxyphenyl)-2-(4-sulfophenyl)-2 H-tetrazolium (MTS) method was used to detect the effect of RL-QN15 on the proliferative activity of HaCaT cells in a high-glucose environment. Cell proliferation activity was assessed using the MTS method 48 h after transfection with the miR-4482-3p mimic, inhibitor and interfering miRNA (NC). The MTS method was also used to detect the effect of RL-QN15 (10 nM) on reversing cell proliferation activity after transfection with miR-4482-3p and NC mimics, with the miR-4482-3p and NC mimic groups without RL-QN15 (10 nM) used as NCs.

Transwell assay

According to our previous study [34], cell migration experiments were performed using Transwell chambers (8-μm pores, Corning Incorporated, USA) to examine the effect of RL-QN15 on HaCaT cell migration ability in a hyperglycemic environment for 48 h. Cell migration ability was assessed using the cell migration assay after transfection with the miR-4482-3p mimic, inhibitor and interfering miRNA (NC) for 48 h. The cell migration assay was utilized to assess the reversal of cell migration ability in the presence of RL-QN15 (10 nM) following transfection with miR-4482-3p and NC mimics, with the miR-4482-3p and NC mimic groups without RL-QN15 (10 nM) used as NCs.

Establishment and administration of diabetic wound model *in vitro*

Male Sprague Dawley rats (n = 80, weighing 180–200 g, aged 5 weeks) were purchased from the Hunan SJA Laboratory Animal Co., Ltd (China). The rats were maintained in separate ventilated cages in the laboratory animal room of Kunming Medical University (Fengshi, China), where they had free access to animal feed and water under a 12 : 12 h light–dark cycle. After 1 week of environmental adaptation, 10 rats were randomly selected as the normal control group and fed a normal pellet diet (NPD), while the other 70 rats were fed a high-fat diet (HFD). After 5 weeks, the NPD group was intraperitoneally injected with sodium citrate buffer solution, while the HFD group was intraperitoneally injected with 0.45% streptozotocin (STZ; 45 mg/kg) containing 0.1 mM sterile sodium citrate buffer solution. After 72 h, blood glucose levels in the rat tails were measured using a blood glucose monitor (ACCU-CHEK Active, Germany). Rats with blood glucose levels ≥16.7 mM/l for 14 consecutive days were considered successfully modeled and used in subsequent experiments.

Next, to establish the foot ulcer model, rats were anesthetized by an intraperitoneal injection of 10% chloral hydrate (Tianjin Chemical Reagent Co., Ltd, China) at a dose of 0.3 ml/100 g. A round full-thickness skin wound (diameter 6 mm) was formed on the back of the hind foot using a 6-mm skin biopsy perforator and Westcott scissors.

The rats were randomly divided into six groups: i.e. normal control, DFU control, RL-QN15 (100 pM), RL-QN15 (1 nM), RL-QN15 (10 nM) and fibroblast growth factor (FGF) (100 ng/ml). From days 0 to 13, the wounds were locally treated with 20 μl of vehicle (PBS), RL-QN15 (100 pM, 1 nM and 10 nM), or FGF (100 ng/ml) twice a day. The

wounds were photographed with a digital camera to obtain images of wound healing on days 0, 3, 7, 10 and 13. ImageJ software was used to calculate healing area at different time points.

Histological analysis

The rats were sacrificed by cervical dislocation on post-operative days 7 and 13 for wound histological analysis. Wound tissues and the surrounding 5-mm area of normal skin were harvested and fixed in 4% formaldehyde, followed by gradient ethanol dehydration, xylene transparency and paraffin embedding. Tissue samples were used for hematoxylin and eosin (H&E), Masson trichrome (MT) and immunofluorescence staining. Sections were viewed and photographed at 4× and 20× fields using a Primovert Microscope (Leica DM4 B, Germany) to obtain images. Images were analyzed and quantified using ImageJ and GraphPad Prism software.

Transcriptomic analysis

To further explore the molecular mechanism underlying the healing effects of the RL-QN15 peptide on DFUs, we designed an *in vitro* diabetic wound model with HaCaT cells. The HaCaT cells were first treated with RL-QN15 (10 nM) for 30 h, with a blank group serving as the NC. The cells were then harvested for transcriptomic and small RNA sequencing analysis (Guoke Biotechnology, China). The sequencing data were then subjected to bioinformatics analysis.

In vitro transfection

Firstly, the hsa-miR-4482-3p mimic, inhibitor and interfering miRNA (NC) were synthesized (GeneCopoeia™, China). Cell transient transfection experiments were performed according to the transfection reagent instructions (EndoFectin™-Max, EF013). HaCaT cells were cultured to 60–70% confluence, and the EndoFectin™-Max transfection reagent and miR-4482-3p mimic, inhibitor and NC were diluted separately with protein-free medium (Opti-MEM® I™). The miR-4482-3p mimic, inhibitor and NC were gently mixed in diluted EndoFectin™-Max transfection reagent and left at room temperature for 5–20 min to allow sufficient formation of the EndoFectin™ complex. The EndoFectin™ complex was gently added to the culture plate drop by drop to spread the culture reagent evenly. The cells are incubated in a CO_2 incubator at 37°C, then harvested after 48 h of transfection and used for further analysis.

Quantitative real-time polymerase chain reaction

An RNAsimple Total RNA Kit (Tiangen, DP419) and miRNA Isolation Kit (Omega, R6842–01, USA) were used to extract total RNA and miRNA from treated HaCaT cells, respectively, according to the protocols provided by the manufacturer. A SureScript™ First-Strand cDNA Synthesis Kit (GeneCopoeia™, QPO56, USA) and BlazeTaq™ SYBR® Green qPCR Mix 2.0 Kit (GeneCopoeia™, QP031, USA) were used to analyze mRNA expression. An All-in-One™ miRNA quantitative real-time polymerase chain reaction (qRT-PCR) Detection System 2.0 Kit (GeneCopoeia™, USA) was used for first-strand cDNA synthesis (miRNA reverse transcription) and qRT-PCR was used for miRNA detection. All-in-One™ miRNA qPCR primer HmiRQP3520 and All-in-One™ qPCR primer HQP054970 (GeneCopoeia, Rockville, USA) were used to detect hsa-miR-4482-3p and VEGFB, and to calculate mRNA and miRNA expression relative to the endogenous control gene glyceraldehyde-3-phosphate dehydrogenase (GAPDH) and U6 small nuclear RNA.

Western blot analysis

The expression levels of VEGFB, p38, p-p38, smad3, p-smad3 and GAPDH were determined by western blot analysis. Total protein was extracted from treated HaCaT cells, quantified using a BCA Protein Assay Kit, then denatured with sodium dodecyl-sulfate polyacrylamide gel electrophoresis protein loading buffer at high temperature. Proteins were separated using 10–12% sodium dodecyl-sulfate polyacrylamide gel electrophoresis and the isolated proteins were then transferred to polyvinylidene fluoride membranes. After blocking with 5% skim milk powder for 1 h, the membranes were incubated with primary antibodies VEGFB (1 : 1000, Invitrogen, ABPA5–116113, USA), p38 (1 : 1000, CST,4511S, USA), p-p38 (1 : 1000, CST, 8690S, USA), smad3 (1 : 1000, CST, ab9523T, USA), p-smad3 (1 : 1000, CST, ab9520S, USA) and GAPDH (1 : 1000, Solarbio, abK20057M, China) overnight at 4°C. After washing three times with Tris-HCl buffer (Solarbio, T1086, China) containing 0.1% Tween-20, the membranes were incubated with secondary antibodies for 1 h at 37°C. The protein bands were visualized using enhanced chemiluminescence substrate reagent (Biosharp, BL520B, China). The gray value of proteins was measured using ImageJ software for quantitative analysis.

Dual-luciferase reporter gene assay

Based on TargetScan and miRDB analysis, VEGFB was predicted as the direct target of miR-4482-3p, with potential specific binding sites between the VEGFB gene sequence and the miR-4482-3p sequence. Target vectors h-VEGFB-3UTR-wt and h-VEGFB-3UTR-mu were constructed first (synthesized by Hanbio Biotechnology Co., Ltd, Shanghai). Next, DMEM (10 μl) was mixed with 0.16 μg of h-VEGFB-3UTR target plasmid and 5 pmol of hsa-miR-4482-3p/NC and placed at room temperature (solution A). After that, DMEM (10 μl) was thoroughly mixed with 0.3 μl of transfection reagent (Hanbio product, concentration 0.8 mg/ml) (solution B) and placed at room temperature for 5 min. Solutions A and B were thoroughly mixed, placed at room temperature for 20 min, and then co-transfected into 293 T cells. After 6 h of transfection, the medium was replaced with fresh medium, and the cells were collected 48 h after transfection

for gene detection (Promega Dual-Luciferase System). The Renilla luciferase value was measured and recorded as the reporter gene luminescence value.

Statistical analysis

All data are presented as mean ± standard deviation and were statistically analyzed using GraphPad Prism v7.0. The Shapiro–Wilk test was used to verify the normality of the data. Student's *t*-tests were employed for comparing two groups when the data followed a normal distribution, while the Mann–Whitney *U* test was used for abnormal distribution. Statistical analysis of multiple groups was conducted using one-way or two-way analysis of variance, followed by *post hoc* tests with Bonferroni correction. $P < 0.05$ was considered statistically significant, and all experiments were performed in triplicate.

Results

RL-QN15 significantly improves HaCaT cell migration and proliferation in a high-glucose environment

To explore the pro-wound repair activity of RL-QN15 *in vitro*, HaCaT cells were cultured with DMEM containing 25 mM glucose for 48 h to simulate a hyper-glucose environment. Cells cultured with glucose-free DMEM were used as a normal control. The ability of RL-QN15 to promote HaCaT cell migration and proliferation under high-glucose conditions was tested using a cell scratch assay, proliferation assay and Transwell migration assay (Figure 1). Based on the wound healing assay, the ability of HaCaT cells to repair scratches after exposure to high glucose (25 mM) was significantly reduced compared to the normal control. However, after RL-QN15 treatment (different concentration gradients), the scratch repair ability of HaCaT cells increased in a concentration- and time-dependent manner (Figure 1a–c). The cell migration assay showed that HaCaT cell migration was significantly reduced in a high-glucose environment, while RL-QN15 improved HaCaT cell migration in a concentration-dependent manner in the same environment (Figure 1d, e), consistent with the wound scratch results. The MTS assay also showed that RL-QN15 promoted HaCaT cell proliferation in a concentration-dependent manner (Figure 1f). Thus, high glucose (25 mM) significantly inhibited HaCaT cell migration and proliferation, while RL-QN15 significantly improved both and maintained normal physiological function of keratinocytes in a high glucose environment.

RL-QN15 significantly promotes DFU healing in rats

Next, we investigated the effects of RL-QN15 on wound healing *in vivo* using a DFU rat model. Changes in body weight were monitored during the modeling process. Compared with the NPD group, HFD rats showed an increase in body weight from week 2. Percentage weight gain continued until the onset of diabetes (week 5 of HFD feeding). After STZ injection, the HFD rats lost weight, while the NPD control group continued to gain weight (Figure 2a). Changes in blood glucose were monitored on days 3, 7 and 13 after STZ injection. The blood glucose level in the DFU group was ≥16.7 mM/l over 14 consecutive days, indicating successful establishment of the model (Figure 2b). The modeling success rate was 82.8% (58/70).

We next evaluated the effects of RL-QN15 on wound healing by creating full-thickness skin wounds on the back of the hind foot of rats, with an equal volume of PBS and local administration of RL-QN15 (different concentration gradients). Foot wound healing in DFU rats was observed on days 0, 3, 7, 10 and 13 after successful modeling. Based on general appearance, wound healing speed in the DFU control group was significantly slower than that in the normal control group. However, DFU healing significantly improved after treatment with RL-QN15 (different concentration gradients) (Figure 2c, d). Currently, FGF has been developed as an effective drug for clinical treatment of wound healing, and thus was used as a positive control in our study. Notably, in the DFU rat model, RL-QN15 (10 nM) showed a better effect on wound healing than FGF (100 ng/ml). Thus, RL-QN15 significantly accelerated the healing process of DFUs in a concentration- and time-dependent manner.

Effect of RL-QN15 on histopathological changes in DFU healing process

Granulation tissue formation, re-epithelialization, collagen deposition and angiogenesis are all signs of wound healing. In this study, we performed histological examination of samples collected on days 7 and 13 to observe the accelerating effect of RL-QN15 treatment on wound healing. On day 7 of treatment, H&E staining analysis (Figure 3a) showed little granulation tissue or re-epithelialization in the DFU control group, whereas thicker granulation tissue with moderate re-epithelialization was observed in the RL-QN15-treated group (Figure 3b, c). On day 13 of treatment, the RL-QN15-treated group showed nearly complete re-epithelization with thinner granulation and epidermal thickness compared with the DFU control group (Figure 3d, e).

MT staining was performed to assess collagen deposition at the wound site (Figure 3f). Almost no collagen formation was observed in the DFU control group on day 7, whereas collagen deposition had begun in the RL-QN15-treated group. On day 13, sparse collagen fibers and unclear tissue structure were observed in the DFU control group, whereas collagen formation was clearly observed and collagenous bundles were arranged in a dense and orderly manner in the RL-QN15-treated group.

Next, to examine the effect of RL-QN15 on angiogenesis, immunofluorescence staining with anti-CD31 antibody (Abcam, ab281583, UK) was employed. As shown in Figure 3g, after 7 days of treatment, the DFU control group exhibited almost no angiogenesis, whereas the RL-QN15-treated group displayed early signs of angiogenesis. By day 13 of treatment, the DFU control group exhibited

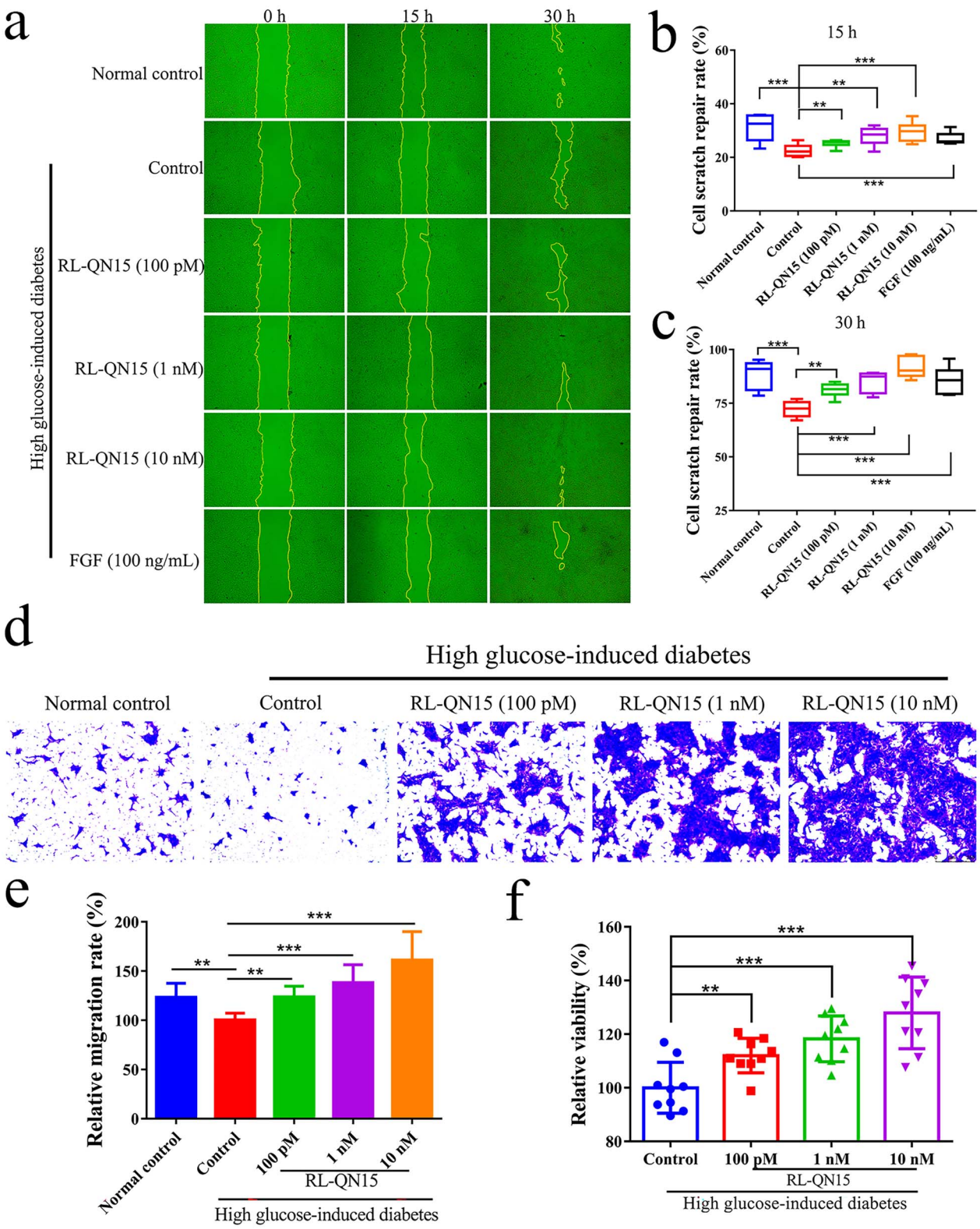

Figure 1. RL-QN15 significantly improves HaCaT cell migration and proliferation in a high-glucose environment. (**a**) Scratch repair activity of RL-QN15 on HaCaT cells in a high-glucose environment, detected by cell scratch assay. (**b**) Healing rate of cell scratches at 15 h. (**c**) Healing rate of cell scratches at 30 h. (**d**) Migration assay was performed to detect effects of RL-QN15 on migration ability of HaCaT cells in a high-glucose environment. (**e**) Relative mobility analysis diagram of HaCaT cells in a high-glucose environment by RL-QN15. (**f**) Cell proliferation assay was used to detect effects of RL-QN15 on the proliferation activity of HaCaT cells in a high-glucose environment. Data are presented as mean ± standard deviation, n = 9; $^{**}p < 0.01$, $^{***}p < 0.005$ (*t*-test). *HaCaT* human immortalized keratinocyte, *FGF* fibroblast growth factor

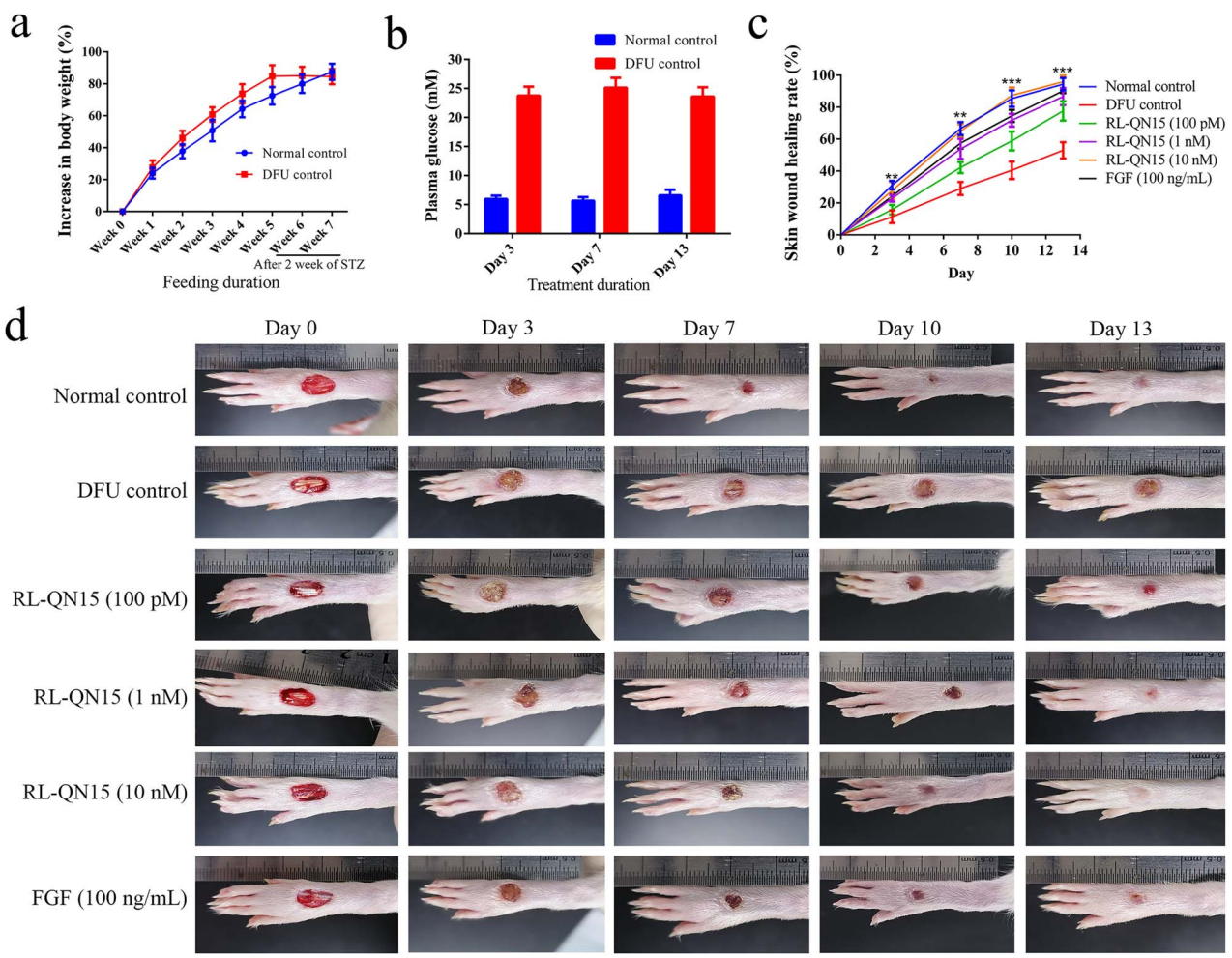

Figure 2. RL-QN15 significantly promotes wound healing in DFU rats. (**a**) Curve of changes in body weight. (**b**) Monitoring of blood glucose levels. (**c**) Healing curves of each group for total cortical wounds. (**d**) Representative graph of wound healing in DFU rat model. Data are presented as mean ± standard deviation, n = 9; $^{**}p < 0.01$, $^{***}p < 0.005$ (*t*-test). *FGF* fibroblast growth factor, *DFU* diabetic foot ulcer

a reduced number of blood vessels, whereas the RL-QN15-treated group showed a significant increase in the number of blood vessels.

Thus, these results suggest that RL-QN15 accelerated wound healing by promoting re-epithelialization and vascular regeneration.

RL-QN15 promotes keratinocyte migration and proliferation by activating p38MAPK and smad3 signaling pathway to inhibit miR-4482-3p expression

To further investigate the mechanism underlying the effects of RL-QN15 on DFU healing, we collected treated HaCaT cells for transcriptomic and small RNA sequencing analysis. Using edgeR software for differential screening, we identified nine up-regulated and 51 down-regulated miRNAs (fold change > = 2 and $p < 0.05$) (Figure S1 a, b, see online supplementary material). We focused on one of the most down-regulated miRNAs, i.e. hsa-miR-4482-3p, whose function in promoting diabetic wound healing has not been investigated. We performed qRT-PCR on treated HaCaT cells and confirmed that miR-4482-3p expression was up-regulated in the high-glucose-treated HaCaT cells compared with normal control, but the expression level of miR-4482-3p was down-regulated in a concentration-dependent manner after RL-QN15 treatment (Figure 4a).

We next explored the signaling pathways mediating the pro-wound repair effects of miR-4482-3p on keratinocytes. Based on the Kyoto Encyclopedia of Genes and Genomes pathway enrichment analysis (Figure S1 c, d, see online supplementary material), we selected the classical p38MAPK and smad3 signaling pathways among the mitogen-activated protein kinase (MAPK) and transforming growth factor-β (TGF-β) signaling pathways related to the promotion of cell proliferation and migration. Western blot analysis showed that the phosphorylation levels of p38MAPK and smad3 in the high-glucose treatment group were significantly lower than those in the normal control group but increased in a concentration-dependent manner after RL-QN15 treatment (Figure 4b, c). In addition, we used the specific p38MAPK inhibitor SB203580 and smad3 inhibitor (E)-SIS3 to investigate the relationship between miR-4482-3p and the p38MAPK and smad3 signaling pathways.

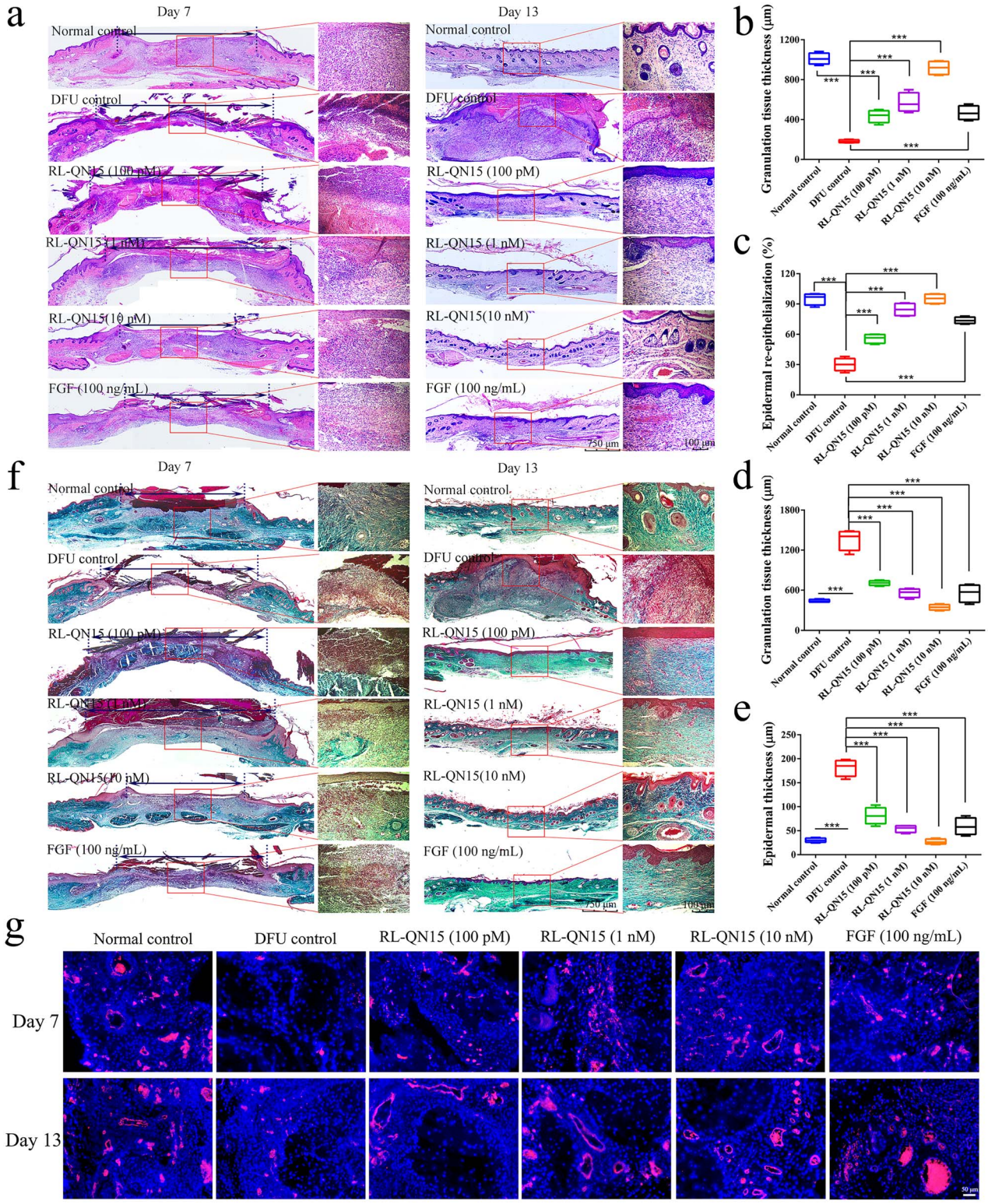

Figure 3. Histological analysis of wounds in DFU rats. (**a**) Representative images of H&E staining on postoperative days 7 and 13 (blue double-ended arrows represent distance between wound edges). Scale bars: 750 μm (left) and 100 μm (right). (**b**) Quantification map of granulation tissue thickness on postoperative day 7. (**c**) Quantitative map of tissue re-epithelialization on postoperative day 7. (**d**) Quantification of granulation tissue thickness on postoperative day 13. (**e**) Quantification of epidermal thickness on postoperative day 13. (**f**) Representative images of MT staining on postoperative days 7 and 13 (blue double-ended arrows represent distance between wound edges). Scale bars: 750 μm (left) and 100 μm (right). (**g**) Immunofluorescence staining used anti-CD31 antibody to identify vascular regeneration. Data are presented as mean ± standard deviation, n = 9; $^{***}p < 0.005$ (*t*-test). *FGF* fibroblast growth factor, *DFU* diabetic foot ulcer, *H&E* hematoxylin and eosin

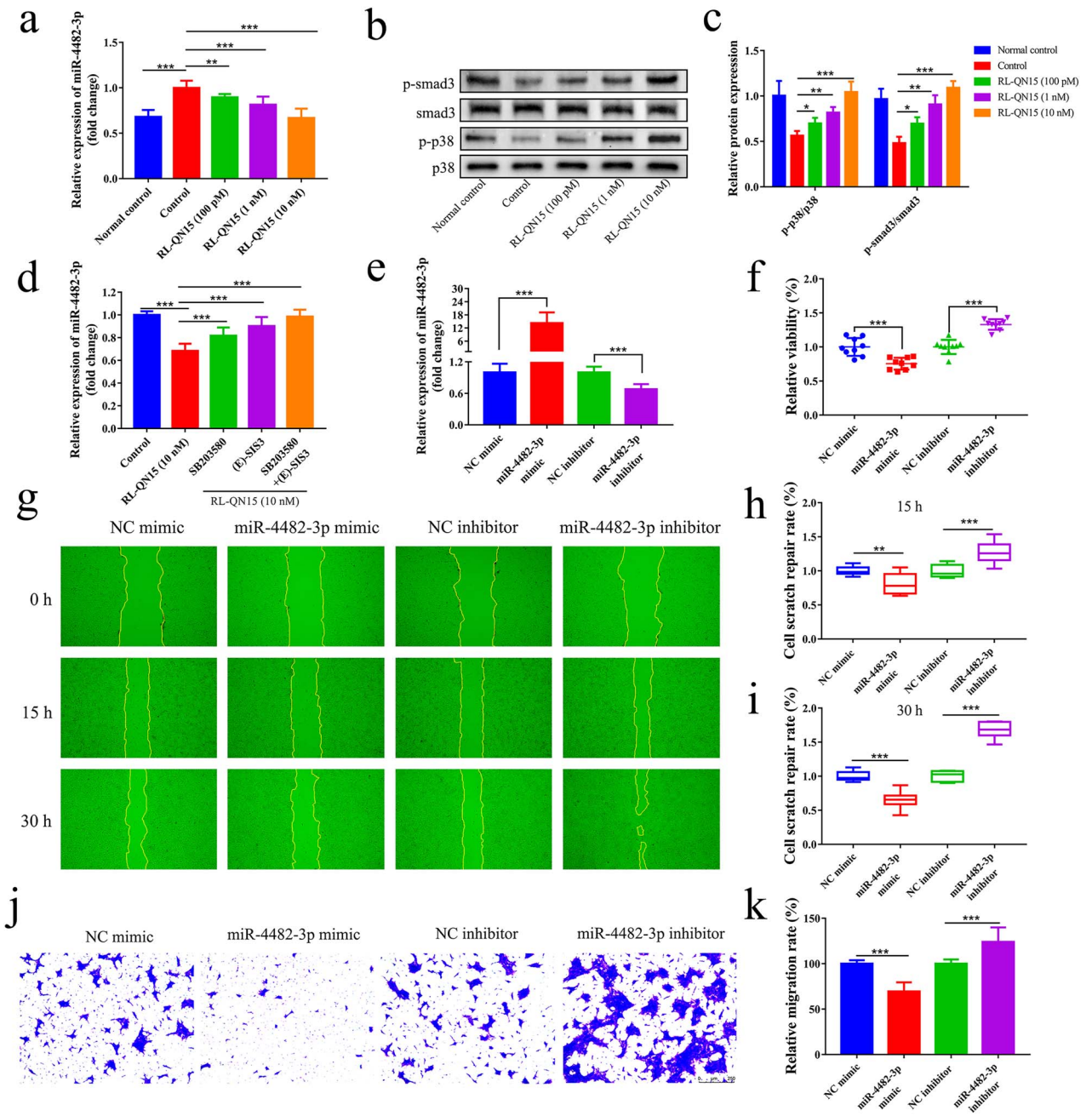

Figure 4. RL-QN15 promotes keratinocyte migration and proliferation by activating p38MAPK and smad3 signaling pathways to inhibit miR-4482-3p expression. (**a**) Expression of miR-4482-3p in HaCaT cells of each group detected by qRT-PCR (n = 9). (**b**) Protein binding map of p38MAPK and smad3 phosphorylation in HaCaT cells determined by western blot analysis. (**c**) Phosphorylation of p38MAPK and smad3 in HaCaT cells determined by western blot analysis (n = 6). (**d**) HaCaT cells were pretreated with SB203580 (10 μm) and (E)-SIS3 (1 μm) for 1 h, then stimulated with RL-QN15 (10 nM) for 24 h. Expression of miR-4482-3p detected by qRT-PCR (n = 9). (**e**) Transfection rate of miR-4482-3p detected by qRT-PCR (n = 9). (**f**) Effect of miR-4482-3p transfection on proliferation of HaCaT cells detected by cell proliferation assay (n = 9). (**g**) Effect of miR-4482-3p transfection on scratch repair ability of HaCaT cells detected by cell scratch assay. (**h**, **i**) Wound healing rate of HaCaT cells at 15 and 30 h after miR-4482-3p transfection (n = 9). (**j**) Effect of miR-4482-3p transfection on migration ability of HaCaT cells detected by cell migration assay. (**k**) Analysis of effect of miR-4482-3p transfection on mobility of HaCaT cells (n = 9). Data are presented as mean ± standard deviation; $^{*}p < 0.05$, $^{**}p < 0.01$, $^{***}p < 0.005$ (*t*-test). *NC* negative control, *HaCaT* human immortalized keratinocyte, *qRT-PCR* quantitative real-time polymerase chain reaction, *p38MAPK* p38 mitogen-activated protein kinase

Pretreatment of HaCaT cells with these agents prevented RL-QN15-mediated down-regulation of miR-4482-3p, with the blocking effect more obvious when the two inhibitors were combined (Figure 4d). These results indicate that RL-QN15 regulates miR-4482-3p expression, partially via activation of the p38MAPK and smad3 signaling pathways.

To investigate the role of miR-4482-3p in cellular processes involved in wound healing, keratinocytes were treated with the miR-4482-3p mimic and inhibitor. Transfection efficiency was detected by qRT-PCR. As shown in Figure 4e, miR-4482-3p expression was increased in keratinocytes transfected with the miR-4482-3p mimic but decreased in

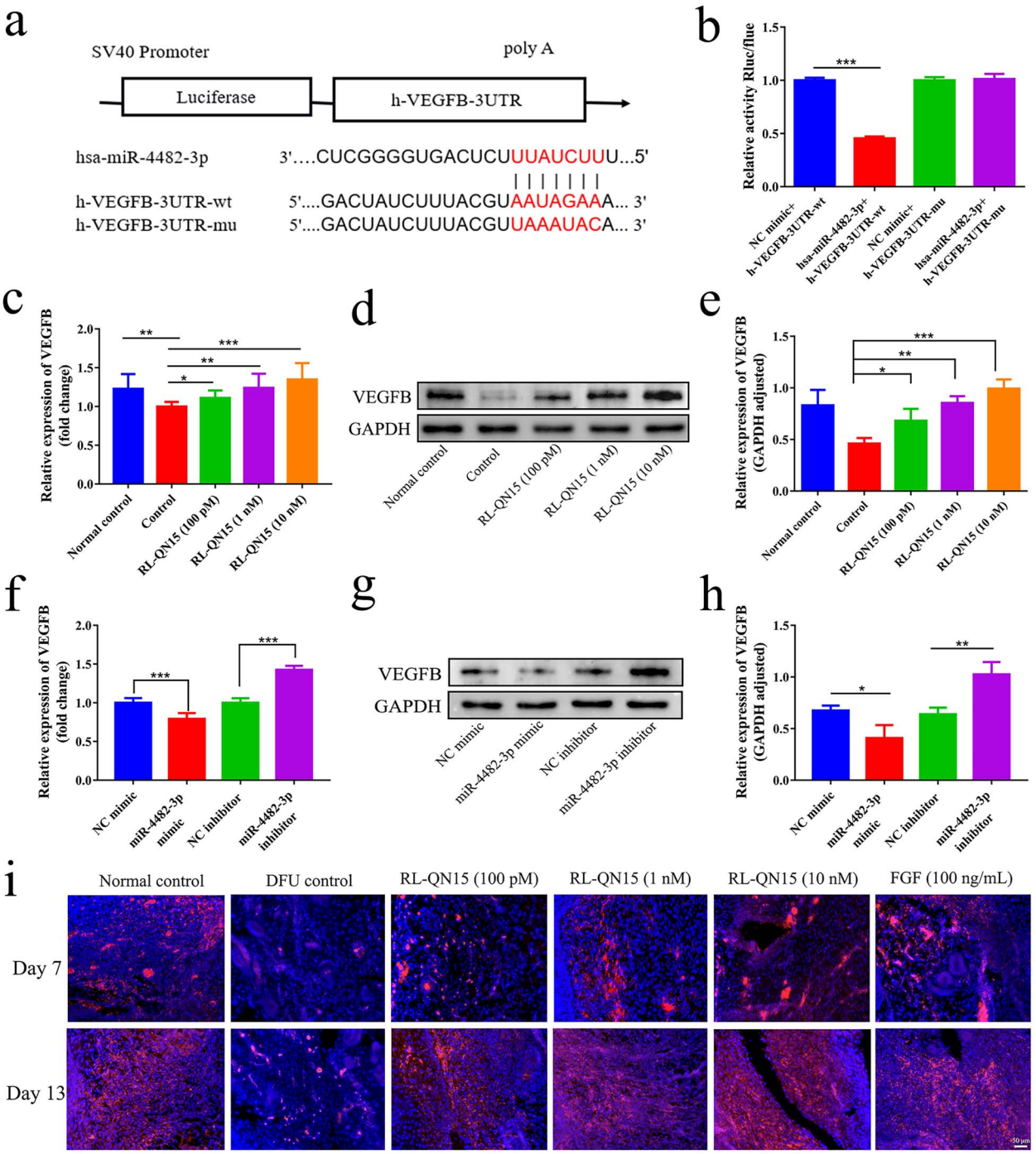

Figure 5. RL-QN15 increases VEGFB production in keratinocytes by inhibiting miR-4482-3p expression. (**a**) Schematic diagram of hsa-miR-4482-3p binding to h-VEGFB-3UTR target sites. (**b**) Dual luciferase reporter gene detection of interaction between hsa-miR-4482-3p and h-VEGFB-3UTR. (**c**) Expression levels of VEGFB mRNA in HaCaT cells of each group determined by qRT-PCR (n = 9). (**d**) Protein binding map of VEGFB protein expression in HaCaT cells determined by western blot analysis. (**e**) Relative protein expression levels of VEGFB normalized to GAPDH in HaCaT cells determined by western blot analysis (n = 6). (**f**) Expression level of VEGFB mRNA in HaCaT cells transfected with miR-4482-3p determined by qRT-PCR (n = 9). (**g**) Protein binding diagram of VEGFB protein expression level in HaCaT cells transfected with miR-4482-3p determined by western blot analysis. (**h**) Relative protein expression level of VEGFB normalized to GAPDH in transfected HaCaT cells determined by western blot analysis (n = 6). (**i**) Representative images of VEGFB immunofluorescence staining in DFU rat model on days 7 and 13 after surgery (×20). Data are presented as mean ± standard deviation; $^{*}p < 0.05$, $^{**}p < 0.01$, $^{***}p < 0.005$ (*t*-test). *NC* negative control, *qRT-PCR* quantitative real-time polymerase chain reaction, *VEGFB* vascular endothelial growth factor B, *GAPDH* glyceraldehyde-3-phosphate dehydrogenase, *DFU* diabetic foot ulcer

keratinocytes transfected with the miR-4482-3p inhibitor ($p < 0.05$). Subsequently, changes in keratinocyte migration and proliferation were analyzed by cell proliferation assay (Figure 4f), cell scratch assay (Figure 4g, h, i) and Transwell migration assay (Figure 4j, k). Results showed that inhibiting miR-4482-3p expression significantly promoted HaCaT

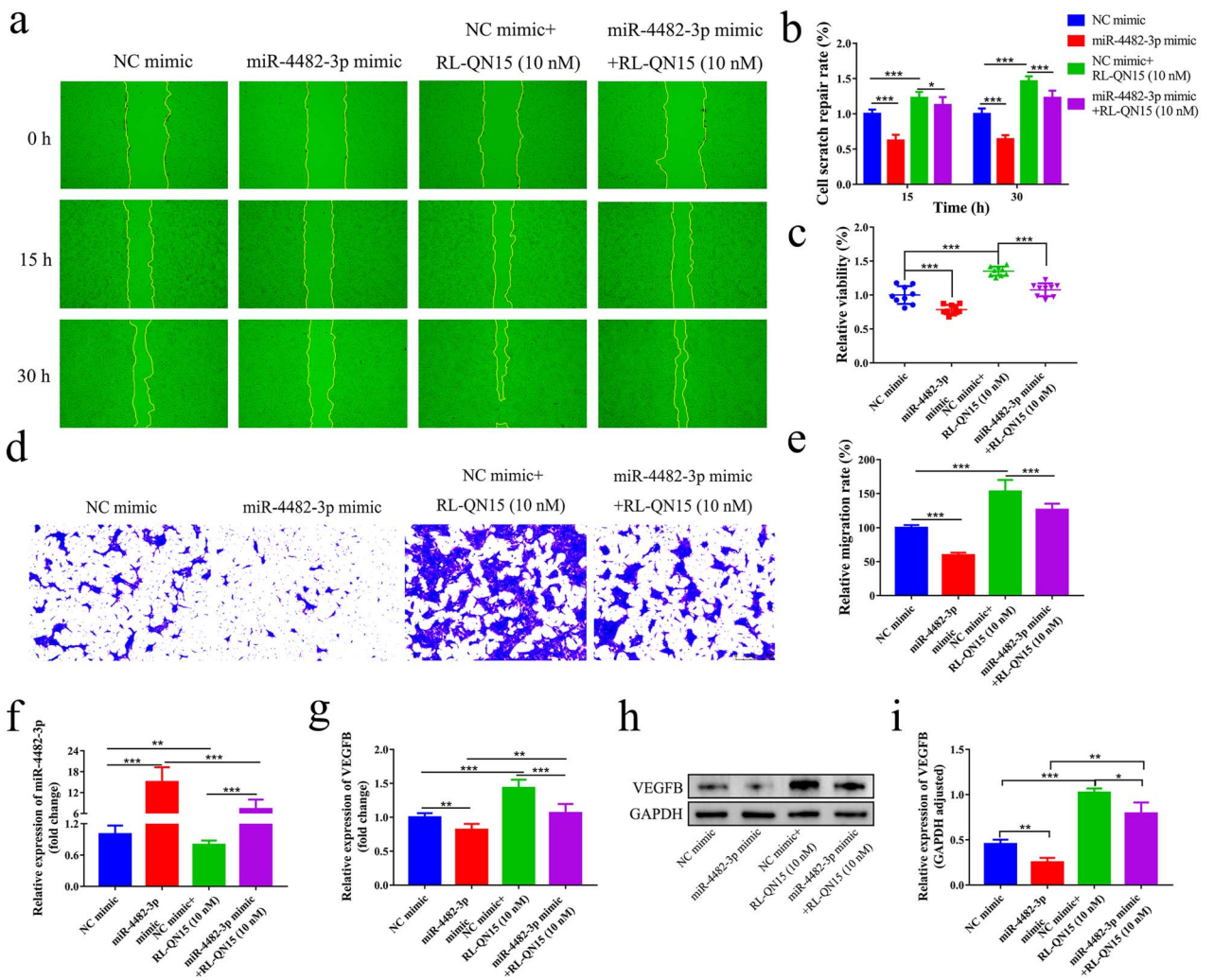

Figure 6. RL-QN15 partially reverses effects of miR-4482-3p mimic on keratinocyte migration and proliferation and VEGFB expression. (**a**) Effect of miR-4482-3p mimic on scratch repair ability of HaCaT cells is partially reversed by RL-QN15 intervention. (**b**) Wound healing rate of HaCaT cells at 15 and 30 h after RL-QN15 intervention (n = 9). (**c**) Effect of miR-4482-3p mimic on proliferation activity of HaCaT cells is partially reversed by RL-QN15 intervention (n = 9). (**d**) Effect of miR-4482-3p mimic on migration ability of HaCaT cells is partially reversed by RL-QN15 intervention. (**e**) Analysis diagram of effects of RL-QN15 intervention on HaCaT cell migration (n = 9). (**f**) qRT-PCR was used to detect expression level of miR-4482-3p in HaCaT cells partially reversed by RL-QN15 intervention (n = 9). (**g**) qRT-PCR was used to detect expression level of VEGFB mRNA in HaCaT cells partially reversed by RL-QN15 intervention (n = 9). (**h**) Protein binding diagram of VEGFB mRNA in HaCaT cells partially reversed by RL-QN15 intervention, determined by western blot analysis. (**i**) Relative protein expression level of VEGFB normalized to GAPDH in HaCaT cells determined by western blot analysis after partial reversal of effects by RL-QN15 intervention (n = 6). Data are presented as mean ± standard deviation; $^{*}p < 0.05$, $^{**}p < 0.01$, $^{***}p < 0.005$ (*t*-test). *NC* negative control, *qRT-PCR* quantitative real-time polymerase chain reaction, *VEGFB* vascular endothelial growth factor B, *GAPDH* glyceraldehyde-3-phosphate dehydrogenase

cell migration and proliferation, whereas overexpression of miR-4482-3p significantly inhibited HaCaT cell migration and proliferation.

These results suggest that RL-QN15 inhibited the expression of miR-4482-3p by activating the p38MAPK and smad3 signaling pathways, thereby promoting the migration and proliferation of keratinocytes.

RL-QN15 increases VEGFB production in keratinocytes by inhibiting miR-4482-3p expression

To understand the regulatory mechanism of miR-4482-3p expression in keratinocytes, TargetScan and miRDB analyses were performed and VEGFB was predicted to be the direct target of miR-4482-3p. For validation, dual luciferase reporter analysis was performed and showed that hsa-miR-4482-3p failed to down-regulate the luciferase expression of h-VEGFB-3UTR-MUT after mutation compared with the NC group ($p > 0.05$), indicating that the mutation was successful. Compared with the NC group, hsa-miR-4482-3p significantly down-regulated luciferase expression of h-VEGFB-3UTR-WT ($p < 0.001$), indicating a potential binding effect between hsa-miR-4482-3p and VEGFB (Figure 5a, b). We next determined the expression of VEGFB by qRT-PCR and western blot analysis and found that the mRNA and protein expression levels of VEGFB were decreased in the high-glucose environment compared with the normal control

group. However, after RL-QN15 treatment, the mRNA and protein expression levels of VEGFB increased in a concentration-dependent manner (Figure 5c, d, e).

We next explored VEGFB expression in keratinocytes treated with the miR-4482-3p mimic and inhibitor by qRT-PCR and western blot analysis. Results showed that keratinocytes transfected with the miR-4482-3p mimic had lower VEGFB mRNA and protein expression levels than keratinocytes transfected with the NC mimic. The opposite trend was found for keratinocytes treated with the miR-4482-3p inhibitor compared with the NC inhibitor. Thus, these results indicate that VEGFB was negatively regulated by miR-4482-3p (Figure 5f, g, h).

Immunofluorescence of wounds in the DFU rat model showed that VEGFB was barely expressed in the DFU control group on day 7 but was detected in the RL-QN15-treated group. On day 13, minor VEGFB expression was observed in the DFU control group, but higher VEGFB expression was observed in the RL-QN15-treated group (Figure 5i).

These results suggest that RL-QN15 accelerated wound healing by promoting vascular regeneration.

RL-QN15 partially reverses effects of miR-4482-3p mimic on keratinocyte migration and proliferation and VEGFB expression

We demonstrated that miR-4482-3p promoted keratinocyte migration and proliferation as well as angiogenesis by targeting the *VEGFB* gene. To further prove that RL-QN15 promotes DFU repair activity by down-regulating miR-4482-3p, we treated keratinocytes with miR-4482-3p mimic and conducted an interference experiment with RL-QN15.

Results showed that RL-QN15 partially reversed the scratch repair ability of HaCaT cells treated with the miR-4482-3p mimic in the cell scratch experiments (Figure 6a, b). The cell proliferation assay results showed that RL-QN15 partially reversed the proliferation ability of HaCaT cells treated with the miR-4482-3p mimic (Figure 6c). The Transwell migration assay results also suggested that RL-QN15 partially reversed the migration ability of HaCaT cells (Figure 6d, e). In addition, qRT-PCR results showed that the expression level of miR-4482-3p was partially reversed in the HaCaT cells treated with RL-QN15 compared with the miR-4482-3p mimetic group (Figure 6f), as was the expression level of VEGFB mRNA (Figure 6g). Western blot results showed that, compared with the miR-4482-3p mimetic group, the expression level of the VEGFB protein was partially reversed after RL-QN15 treatment (Figure 6h, i). Thus, these results suggest that RL-QN15 promoted the repair activity of DFUs by down-regulating miR-4482-3p.

Discussion

Due to their complex pathogenesis, DFUs often result in poor wound healing [4,43]. Current standard practices in DFU management do not meet clinical needs, and DFU treatment remains an extremely challenging task [44–46].

In this study, we identified the role of the RL-QN15 peptide in maintaining physiological function and plasticity of keratinocytes by activating the p38MAPK and smad3 signaling pathways to inhibit miR-4482-3p expression. Furthermore, we found that miR-4482-3p targeted VEGFB to promote VEGF secretion by HaCaT cells, thereby accelerating wound healing.

As the most important cell type in the skin, keratinocytes play a crucial role in promoting wound re-epithelialization and inflammatory to proliferative stage transition during wound healing [8,11,47]. However, a high-glucose environment can interfere with the physiological function of keratinocytes, leading to impaired wound healing in diabetic patients [20,21]. Therefore, maintaining normal physiological function of keratinocytes is beneficial for the healing of DFUs [48]. In this study, we observed that HaCaT cell proliferation and migration abilities were decreased in high-glucose environments but improved after treatment with RL-QN15. *In vivo* experiments using the rat DFU model showed that the wound healing rate of the DFU control group was significantly slower than that of the normal control group, whereas RL-QN15 treatment significantly accelerated the healing process. Histopathological results showed little granulation tissue and re-epithelialization in the DFU control group on day 7, as well as little collagen formation and VEGFB expression. On day 13, granulation tissue in the DFU control group was thickened, indicating that the wound was still in the inflammatory stage. Collagen fibers also remained sparse and poorly organized at the wound site and VEGFB expression was low. In the RL-QN15-treated group, however, re-epithelialization and granulation tissue regeneration were observed on day 7, and collagen deposition and VEGFB expression started to appear. On day 13, re-epithelialization was complete, granulation and epidermal tissues were thinner, collagen was arranged in a dense and orderly manner at the wound site, and VEGFB expression was increased. In addition, immunofluorescence staining of blood vessels revealed that the DFU control group exhibited almost no signs of angiogenesis after 7 days of treatment, while the RL-QN15-treated group displayed early indications of angiogenesis. Furthermore, on day 13, the number of blood vessels increased significantly in the RL-QN15-treatment group compared to the DFU control group. These results indicate that RL-QN15 can promote keratinocyte migration and proliferation during wound healing under a high-glucose environment and can promote angiogenesis at the wound site. Thus, this treatment accelerated the process of wound re-epithelialization and promoted the transition from the inflammatory to the proliferative phase, thus accelerating DFU wound healing.

The role of miRNAs in human diseases has been extensively studied [49,50] and several miRNAs have been implicated in the healing process of diabetic skin wounds [23,27,51]. Therefore, miRNAs are considered as potential therapeutic targets for chronic wounds such as DFUs. In this study, we identified a novel miRNA,

miR-4482-3p, and investigated its expression and function in promoting DFU wound healing. We found that miR-4482-3p expression was up-regulated in high-glucose-induced HaCaT cells compared with the normal control group, whereas miR-4482-3p expression was down-regulated in the RL-QN15 treatment group. We also performed cell transfection experiments using the miR-4482-3p mimic and inhibitor. Results showed that overexpression of miR-4482-3p decreased the migration and proliferation of HaCaT cells in a high-glucose environment, whereas inhibition of miR-4482-3p enhanced HaCaT cell migration and proliferation under high-glucose conditions. We also identified the growth-promoting MAPK and TGF-β signaling pathways based on transcriptomic analysis. Activation of the MAPK and TGF-β signaling pathways has been shown to promote cell proliferation and migration [52–54]. Notably, p38MAPK plays an important role in regulating angiogenic responses [55–57], while smad3 induces the cellular secretion of pro-vascular growth factors [58–60]. Here, results showed that RL-QN15 promoted the phosphorylation of p38MAPK and smad3 in a concentration-dependent manner, whereas treatment with the p38MAPK and smad3 inhibitor reversed RL-QN15-mediated miR-4482-3p expression. These results suggest that RL-QN15 inhibited the expression of miR-4482-3p via activation of the p38MAPK and smad3 signaling pathways, thereby promoting the migration and proliferation of keratinocytes.

Angiogenesis is essential for DFU wound repair [14,15]. Keratinocytes induce angiogenesis at the wound site through VEGF derived during wound healing [61–63]. VEGFB, a member of the VEGF family, is reported to enhance neovascularization in skin wound healing [64]. Our results showed that the expression levels of VEGFB mRNA and protein were down-regulated in HaCaT cells under high-glucose conditions compared with the normal control group but were up-regulated in the RL-QN15 treatment group. The transfection experiments indicated that the expression levels of VEGFB mRNA and protein were down-regulated when miR-4482-3p was overexpressed but were up-regulated when miR-4482-3p expression was inhibited. The dual luciferase reporter assay also showed binding between hsa-miR-4482-3p and VEGFB. Thus, these results suggest that RL-QN15 accelerated wound healing by promoting vascular regeneration.

We next treated the keratinocytes with the miR-4482-3p mimic and interfered with RL-QN15, verifying that RL-QN15 promoted DFU repair activity via down-regulation of miR-4482-3p. Notably, RL-QN15 partially reversed the migratory and proliferative ability of cells treated with miR-4482-3p mimic. At the molecular level, RL-QN15 also partially reversed the expression levels of miR-4482-3p and VEGFB mRNA in cells treated with miR-4482-3p mimic.

Conclusions

In summary, we found that RL-QN15 can promote wound healing and that miR-4482-3p is involved in the healing process of DFUs. Notably, RL-QN15 can restore the physiological function of keratinocytes in high-glucose environments, promote re-epithelialization and angiogenesis at the wound site by promoting keratinocyte migration and proliferation, and accelerate wound healing of DFUs. Thus, this study should provide novel drug candidates and effective therapeutic targets for the clinical treatment of DFUs.

Abbreviations

DFUs: Diabetic foot ulcers; DMEM: Dulbecco's modified Eagle's medium; FGF: Fibroblast growth factor; GAPDH: Glyceraldehyde-3-phosphate dehydrogenase; HaCaT: Human immortalized keratinocyte; H&E: Hematoxylin and eosin; HFD: High-fat diet MAPK: Mitogen-activated protein kinase; miRNA: MicroRNA; MT: Masson trichrome; MTS: 3-(4, 5-Dimethylthiazol-2-yl)-5-(3-carboxymethoxyphenyl)-2-(4-sulfophenyl)-2H-tetrazolium; NC inhibitor: Negative control inhibitor; NC mimic: Negative control mimic; NPD: Normal pellet diet; qRT-PCR: Quantitative real-time polymerase chain reaction; TGF-β: Transforming growth factor-β; MMP9: Matrix metalloprotease 9; SPRY1: Sprout homolog 1; PBS: Phosphate-buffered saline; STZ: Streptozotocin; VEGF: Vascular endothelial growth factor.

Supplementary data

Supplementary data is available at *Burns & Trauma Journal* online.

Acknowledgments

The authors thank their team for helpful comments and technical assistance.

Funding

This work was supported by grants from the National Natural Science Foundation of China (32360138, 32060212, 32301054 and 81760648), Key Program of Yunnan Fundamental Research Project (202301AS070036), Outstanding Youth Program of Yunnan Applied Basic Research Project-Kunming Medical University Union Foundation (202301AY070001-301), Project of Yunnan Applied Basic Research Project-Kunming Medical University Union Foundation (202101AY070001-006 and 202101AY070001-036).

Data availability

The data that support the findings of this study are available from the corresponding author upon reasonable request.

Authors' contributions

X.Y., J.S. and Y.W. supervised the study and provided financial support; D.S. and K.G. analyzed the data and wrote the original draft; N.L., Y.L., S.L., Y.H. and S.L. participated in analyzing data; Z.F., Y.W., Y.Z. and J.L. participated in the *in vivo* experiments; C.L., Z.W., Y.W. and Z.K. participated in the *in vitro* experiments. All authors read and approved the final manuscript.

Conflict of interest

The authors declare that they have no competing interests.

References

1. Sun H, Saeedi P, Karuranga S, Pinkepank M, Ogurtsova K, Duncan BB, *et al.* IDF diabetes atlas: global, regional and country-level diabetes prevalence estimates for 2021 and projections for 2045. *Diabetes Res Clin Pract*. 2022;183:109119.
2. Boulton AJ, Vileikyte L, Ragnarson-Tennvall G, Apelqvist J. The global burden of diabetic foot disease. *Lancet (London, England)*. 2005;366:1719–24.
3. Singh N, Armstrong DG, Lipsky BA. Preventing foot ulcers in patients with diabetes. *JAMA*. 2005;293:217–28.
4. Patel S, Srivastava S, Singh MR, Singh D. Mechanistic insight into diabetic wounds: pathogenesis, molecular targets and treatment strategies to pace wound healing. *Biomedicine & pharmacotherapy = Biomedecine & pharmacotherapie*. 2019;112:108615.
5. Zhu L, Zhong Q, Yang T, Xiao X. Improved therapeutic effects on diabetic foot by human mesenchymal stem cells expressing MALAT1 as a sponge for microRNA-205-5p. *Aging*. 2019;11:12236–45.
6. Tellechea A, Bai S, Dangwal S, Theocharidis G, Nagai M, Koerner S, *et al.* Topical application of a mast cell stabilizer improves impaired diabetic wound healing. *The Journal of investigative dermatology*. 2020;140:901–11.e11.
7. Wei ZR, Jian Y. Discussion on surgical treatment mode of diabetic foot wounds. *Chinese Journal of Burns and Wounds*. 2023;39:305–10.
8. Strbo N, Yin N, Stojadinovic O. Innate and adaptive immune responses in wound epithelialization. *Advances in wound care*. 2014;3:492–501.
9. Pastar I, Stojadinovic O, Yin NC, Ramirez H, Nusbaum AG, Sawaya A, *et al.* Epithelialization in wound healing: a comprehensive review. *Advances in wound care*. 2014;3:445–64.
10. Souren JM, Ponec M, van Wijk R. Contraction of collagen by human fibroblasts and keratinocytes. *vitro cellular & developmental biology: journal of the Tissue Culture Association*. 1989;25:1039–45.
11. Piipponen M, Li D, Landén NX. The immune functions of keratinocytes in skin wound healing. *Int J Mol Sci*. 2020;21:8790.
12. Goren I, Müller E, Schiefelbein D, Gutwein P, Seitz O, Pfeilschifter J, *et al.* Akt1 controls insulin-driven VEGF biosynthesis from keratinocytes: implications for normal and diabetes-impaired skin repair in mice. *The Journal of investigative dermatology*. 2009;129:752–64.
13. Frank S, Hübner G, Breier G, Longaker MT, Greenhalgh DG, Werner S. Regulation of vascular endothelial growth factor expression in cultured keratinocytes. Implications for normal and impaired wound healing. *J Biol Chem*. 1995;270:12607–13.
14. Okonkwo UA, DiPietro LA. Diabetes and wound angiogenesis. *Int J Mol Sci*. 2017;18:1419.
15. Tonnesen MG, Feng X, Clark RA. Angiogenesis in wound healing. *The journal of investigative dermatology Symposium proceedings*. 2000;5:40–6.
16. Yang Z, Hu X, Zhou L, He Y, Zhang X, Yang J, *et al.* Photodynamic therapy accelerates skin wound healing through promoting re-epithelialization. *Burns & trauma*. 2021;9:tkab008.
17. Iyer S, Darley PI, Acharya KR. Structural insights into the binding of vascular endothelial growth factor-B by VEGFR-1(D2): recognition and specificity. *J Biol Chem*. 2010;285:23779–89.
18. Räsänen M, Sultan I, Paech J, Hemanthakumar KA, Yu W, He L, *et al.* VEGF-B promotes endocardium-derived coronary vessel development and cardiac regeneration. *Circulation*. 2021;143:65–77.
19. Silvestre JS, Tamarat R, Ebrahimian TG, Le-Roux A, Clergue M, Emmanuel F, *et al.* Vascular endothelial growth factor-B promotes in vivo angiogenesis. *Circ Res*. 2003;93:114–23.
20. Lan CC, Liu IH, Fang AH, Wen CH, Wu CS. Hyperglycaemic conditions decrease cultured keratinocyte mobility: implications for impaired wound healing in patients with diabetes. *Br J Dermatol*. 2008;159:1103–15.
21. Hu SC, Lan CE. High-glucose environment disturbs the physiologic functions of keratinocytes: focusing on diabetic wound healing. *J Dermatol Sci*. 2016;84:121–7.
22. Wang P, Chen ZH, Jiang LY, Zhou XQ, Jia CY, Xiao HA. Screening, functional analysis and clinical validation of differentially expressed genes in diabetic foot ulcers. *Chinese Journal of Burns and Wounds*. 2022;38:944–51.
23. Goodarzi G, Maniati M, Qujeq D. The role of microRNAs in the healing of diabetic ulcers. *Int Wound J*. 2019;16:621–33.
24. Ambros V. The functions of animal microRNAs. *Nature*. 2004;431:350–5.
25. Bartel DP. MicroRNAs: target recognition and regulatory functions. *Cell*. 2009;136:215–33.
26. Wang W, Yang C, Wang XY, Zhou LY, Lao GJ, Liu D, *et al.* MicroRNA-129 and -335 promote diabetic wound healing by inhibiting Sp1-mediated MMP-9 expression. *Diabetes*. 2018;67:1627–38.
27. Wu Y, Zhang K, Liu R, Zhang H, Chen D, Yu S, *et al.* MicroRNA-21-3p accelerates diabetic wound healing in mice by downregulating SPRY1. *Aging*. 2020;12:15436–45.
28. Yang X, Wang Y, Wu C, Ling EA. Animal venom peptides as a treasure trove for new therapeutics against neurodegenerative disorders. *Curr Med Chem*. 2019;26:4749–74.
29. Henninot A, Collins JC, Nuss JM. The current state of peptide drug discovery: back to the future? *J Med Chem*. 2018;61:1382–414.
30. Zhang Y, Wang QQ, Zhao Z, Deng CJ. Animal secretory endolysosome channel discovery. *Zool Res*. 2021;42:141–52.
31. Hu Y, Meng B, Yin S, Yang M, Li Y, Liu N, *et al.* Scorpion venom peptide HsTx2 suppressed PTZ-induced seizures in mice via the circ_0001293/miR-8114/TGF-β2 axis. *J Neuroinflammation*. 2022;19:284.
32. Sims EK, Carr ALJ, Oram RA, DiMeglio LA, Evans-Molina C. 100 years of insulin: celebrating the past, present and future of diabetes therapy. *Nat Med*. 2021;27:1154–64.
33. Athauda D, Foltynie T. The glucagon-like peptide 1 (GLP) receptor as a therapeutic target in Parkinson's disease: mechanisms of action. *Drug Discov Today*. 2016;21:802–18.
34. Wang Y, Feng Z, Yang M, Zeng L, Qi B, Yin S, *et al.* Discovery of a novel short peptide with efficacy in accelerating the healing of skin wounds. *Pharmacol Res*. 2021;163:105296.
35. Qin P, Meng Y, Yang Y, Gou X, Liu N, Yin S, *et al.* Mesoporous polydopamine nanoparticles carrying peptide RL-QN15 show potential for skin wound therapy. *Journal of nanobiotechnology*. 2021;19:309.
36. Qin P, Tang J, Sun D, Yang Y, Liu N, Li Y, *et al.* Zn(2+) cross-linked alginate carrying hollow silica nanoparticles loaded with RL-QN15 peptides provides promising treatment for chronic skin wounds. *ACS Appl Mater Interfaces*. 2022;14:29491–505.
37. Sun H, Wang Y, He T, He D, Hu Y, Fu Z, *et al.* Hollow polydopamine nanoparticles loading with peptide RL-QN15: a

new pro-regenerative therapeutic agent for skin wounds. *Journal of nanobiotechnology*. 2021;19:304.
38. Liu N, Li Y, Yang Y, Shu L, Liu Y, Wu Y, *et al*. OL-FS13 alleviates experimental cerebral ischemia-reperfusion injury. *Exp Neurol*. 2022;357:114180.
39. Yin S, Pang A, Liu C, Li Y, Liu N, Li S, *et al*. Peptide OM-LV20 protects astrocytes against oxidative stress via the 'PAC1R/JNK/TPH1' axis. *J Biol Chem*. 2022;298:102429.
40. Li Y, Jin T, Liu N, Wang J, Qin Z, Yin S, *et al*. A short peptide exerts neuroprotective effects on cerebral ischemia-reperfusion injury by reducing inflammation via the miR-6328/IKKβ/NF-κB axis. *J Neuroinflammation*. 2023;20:53.
41. Fu Z, Sun H, Wu Y, Li C, Wang Y, Liu Y, *et al*. A cyclic heptapeptide-based hydrogel boosts the healing of chronic skin wounds in diabetic mice and patients. *NPG Asia Materials*. 2022;14:99.
42. Zhang Y, Wang Y, Zeng L, Liu Y, Sun H, Li S, *et al*. Amphibian-derived peptide homodimer OA-GL17d promotes skin wound regeneration through the miR-663a/TGF-β1/Smad axis. *Burns & trauma*. 2022;10:tkac032.
43. Baltzis D, Eleftheriadou I, Veves A. Pathogenesis and treatment of impaired wound healing in diabetes mellitus: new insights. *Adv Ther*. 2014;31:817–36.
44. Everett E, Mathioudakis N. Update on management of diabetic foot ulcers. *Ann N Y Acad Sci*. 2018;1411:153–65.
45. Zubair M, Ahmad J. Role of growth factors and cytokines in diabetic foot ulcer healing: a detailed review. *Rev Endocr Metab Disord*. 2019;20:207–17.
46. Game FL, Apelqvist J, Attinger C, Hartemann A, Hinchliffe RJ, Löndahl M, *et al*. Effectiveness of interventions to enhance healing of chronic ulcers of the foot in diabetes: a systematic review. *Diabetes Metab Res Rev*. 2016;32:154–68.
47. Ren H, Zhao F, Zhang Q, Huang X, Wang Z. Autophagy and skin wound healing. *Burns & trauma*. 2022;10:tkac003.
48. Zhang J, Yang P, Liu D, Gao M, Wang J, Yu T, *et al*. Inhibiting hyper-O-GlcNAcylation of c-Myc accelerate diabetic wound healing by alleviating keratinocyte dysfunction. *Burns & trauma*. 2021;9:tkab031.
49. Mendell JT, Olson EN. MicroRNAs in stress signaling and human disease. *Cell*. 2012;148:1172–87.
50. Slack FJ, Chinnaiyan AM. The role of non-coding RNAs in oncology. *Cell*. 2019;179:1033–55.
51. Ban E, Jeong S, Park M, Kwon H, Park J, Song EJ, *et al*. Accelerated wound healing in diabetic mice by miRNA-497 and its anti-inflammatory activity. *Biomedicine & pharmacotherapy = Biomedecine & pharmacotherapie*. 2020;121:109613.
52. Cuadrado A, Nebreda AR. Mechanisms and functions of p38 MAPK signalling. *The Biochemical journal*. 2010;429:403–17.
53. Chen X, Chen J. miR-3188 regulates cell proliferation, apoptosis, and migration in breast cancer by targeting TUSC5 and regulating the p38 MAPK Signaling pathway. *Oncol Res*. 2018;26:363–72.
54. Song T, Zhao J, Jiang T, Jin X, Li Y, Liu X. Formononetin protects against balloon injury-induced neointima formation in rats by regulating proliferation and migration of vascular smooth muscle cells via the TGF-β1/Smad3 signaling pathway. *Int J Mol Med*. 2018;42:2155–62.
55. McMullen M, Keller R, Sussman M, Pumiglia K. Vascular endothelial growth factor-mediated activation of p38 is dependent upon Src and RAFTK/Pyk2. *Oncogene*. 2004;23:1275–82.
56. Han SW, Jung YK, Lee EJ, Park HR, Kim GW, Jeong JH, *et al*. DICAM inhibits angiogenesis via suppression of AKT and p38 MAP kinase signalling. *Cardiovasc Res*. 2013;98:73–82.
57. Wu G, Luo J, Rana JS, Laham R, Sellke FW, Li J. Involvement of COX-2 in VEGF-induced angiogenesis via P38 and JNK pathways in vascular endothelial cells. *Cardiovasc Res*. 2006;69:512–9.
58. Petersen M, Pardali E, van der Horst G, Cheung H, van den Hoogen C, van der Pluijm G, *et al*. Smad2 and Smad3 have opposing roles in breast cancer bone metastasis by differentially affecting tumor angiogenesis. *Oncogene*. 2010;29:1351–61.
59. Kobayashi T, Liu X, Wen FQ, Fang Q, Abe S, Wang XQ, *et al*. Smad3 mediates TGF-beta1 induction of VEGF production in lung fibroblasts. *Biochem Biophys Res Commun*. 2005;327:393–8.
60. Sun H, Miao C, Liu W, Qiao X, Yang W, Li L, *et al*. TGF-β1/TβRII/Smad3 signaling pathway promotes VEGF expression in oral squamous cell carcinoma tumor-associated macrophages. *Biochem Biophys Res Commun*. 2018;497:583–90.
61. Brown LF, Yeo KT, Berse B, Yeo TK, Senger DR, Dvorak HF, *et al*. Expression of vascular permeability factor (vascular endothelial growth factor) by epidermal keratinocytes during wound healing. *J Exp Med*. 1992;176:1375–9.
62. Kahlina K, Goren I, Pfeilschifter J, Frank S. p68 DEAD box RNA helicase expression in keratinocytes. Regulation, nucleolar localization, and functional connection to proliferation and vascular endothelial growth factor gene expression. *J Biol Chem*. 2004;279:44872–82.
63. Schiefelbein D, Goren I, Fisslthaler B, Schmidt H, Geisslinger G, Pfeilschifter J, *et al*. Biphasic regulation of HMG-CoA reductase expression and activity during wound healing and its functional role in the control of keratinocyte angiogenic and proliferative responses. *J Biol Chem*. 2008;283:15479–90.
64. Mould AW, Greco SA, Cahill MM, Tonks ID, Bellomo D, Patterson C, *et al*. Transgenic overexpression of vascular endothelial growth factor-B isoforms by endothelial cells potentiates postnatal vessel growth in vivo and in vitro. *Circ Res*. 2005;97:e60–70.